An Approach to the Quantitative Assessment of Retinal Layer Distortions and Subretinal Fluid in SD-OCT Images*

Melinda Katona[a] and László G. Nyúl[a]

Abstract

A modern tool for age-related macular degeneration (AMD) investigation is Optical Coherence Tomography (OCT), which can produce high resolution cross-sectional images of retinal layers. AMD is one of the most frequent reasons for blindness in economically developed countries. AMD means degeneration of the macula, which is responsible for central vision. Since AMD affects only this specific part of the retina, untreated patients lose their fine shape- and face recognition, reading ability, and central vision. Here, we deal with the automatic localization of subretinal fluid areas and also analyze retinal layers, since layer information can help to localize fluid regions. We present an algorithm that automatically delineates the two extremal retinal layers, successfully localizes subretinal fluid regions, and computes their extent. We present our results using a set of SD-OCT images. The quantitative information can also be visualized in an anatomical context for visual assessment.

Keywords: optical coherence tomography, SD-OCT, age-related macular degeneration, AMD, subretinal fluid, retinal layer segmentation

1 Introduction

Age-related macular degeneration is one of the most frequent reasons for blindness in economically developed countries. In the world, more and more people suffer from AMD, which presents a challenge to the health systems. AMD means degeneration of the macula which is responsible for central vision. Since AMD affects only this specific part of the retina, untreated patients lose their fine shape- and face recognition, reading ability, and central vision [11].

In essence, AMD has two forms, namely dry and wet form, and the latter causes fast and serious visual impairment in 10% of the cases [14]. In this type of disease, abnormal angiogenesis starts from the choroid under the macula. Fluid and blood leak out of the neovascularized membrane to retina layers, and this ruins the photoreceptors.

Experiments have demonstrated that the vascular endothelial growth factor (VEGF) plays a vital role in the formation of choroidal neovascularization [5]. Currently, the most common and effective clinical treatment for wet AMD is anti-VEGF therapy, which is a periodic intravitreal (into the eye) injection [12].

In the last decade, Optical Coherence Tomography (OCT) has been widely used in the diagnosis of AMD and follow-up therapy. Spectral domain OCT (SD-OCT) produces 3D image volumes, which have been useful in clinical practice. Existing OCT systems are partially suited to monitoring the progress of the disease, but OCT reveals many features about AMD such as hyper-reflective dots (HRD), subretinal fluid and cysts. Figure 1 presents an SD-OCT B-scan with biomarkers of AMD.
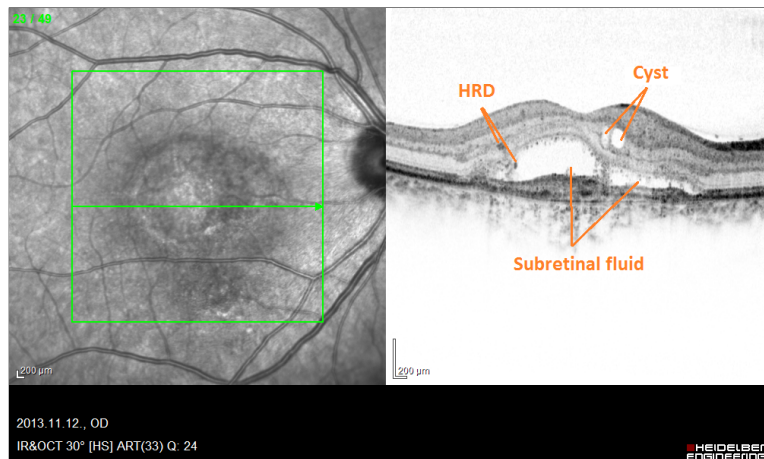

Figure 1: Original Optical Coherence Tomography (SD-OCT) image with biomarkers of AMD.

In the literature, a large number of publications exist on detecting retinal layers based on various techniques. One approach is the automatic segmentation procedure using graph theory [1, 2, 8]. In this approach, the graph nodes usually relate to image pixels, the graph edges are assigned to pairs of pixels, and the edge weights depend on the intensity differences between the two pixels, and also may depend on spatial distance between the pixels. Image segmentation then becomes a graph cutting problem, which can be handled by dynamic programming. These approaches are less tolerant to noise, which is a disadvantage, because images are often very noisy. Another basic idea relies on the well-known energy-minimizing active contour method which, unfortunately, cannot handle low contrast and noise.

Yazdanpanah et al. [21] suggested a multi-phase framework with a circular shape prior for modeling the boundaries of retinal layers and estimating the shape parameters. They used a contextual scheme to balance the weights of different terms in the energy functional. Also, machine learning has been widely used in recent years for retinal image analysis. Lang et al. [13] used a random forest classifier to segment retinal layers. The random forest classifier learns the boundary pixels between layers and produces an accurate probability map for each boundary, which is further processed to finalize boundaries. Procedures based on active contour or machine learning provide an effective solution, but these methods are too time-consuming. Hassan et al. [10] used a structure tensor approach combined with a nonlinear diffusion process for layer detection. A structure tensor is a second-moment matrix that displays similarities and prominent orientations of the image gradient. Some other approaches use optimized boundary tracking [7] or polynomial smoothing [15]. These algorithms are rather complex.

Many studies focus on automatic detection of subretinal fluid in OCT images. One of the most popular approaches is based on the Split-Bregman optimization technique [9]. This method is used to segment dark regions (depending on the image acquisition settings) between layers. These segmented regions are treated as possible fluid candidates. A random forest classifier is trained to distinguish true fluid regions from false segments [3, 22]. Also, a fuzzy level set method was introduced by Wang et al. [19] to identify fluid-filled regions. They use the combination of three types of scans (two types of B-scans and a C-scan) to generate a comprehensive volumetric segmentation of the retinal fluid. The remaining artifacts are removed by identifying morphological characteristics and vascular shadowing. Novosel et al. [16] recommended a locally-adaptive loosely-coupled level set method. This approach exploits the local attenuation coefficient differences of layers around an interface to delineate the fluid. This concept can also handle abrupt attenuation coefficient variations and topology-disrupting anomalies. SEAD (symptomatic exudate-associated derangements) segmentation in 3D volumes plays and important role in the treatment of neovascular AMD. The accurate detection is a challenge because of the large diversity of SEAD size, location and shape. Xu et al. [20] proposed a voxel classification-based approach using a layer-dependent stratified sampling strategy to address the class imbalance problem in SEAD detection.

In this paper, we deal with the automatic localization of subretinal fluid areas and also analyze retinal layers, since layer information can help to localize fluid regions. We present an algorithm that automatically delineates the ILM (inner-limiting membrane) and RPE (retinal pigment epithelium) retinal layers, successfully localizes subretinal fluid regions, and computes their extent. We present our results using a set of SD-OCT images and we depict our results in two different ways. Our proposed method is based on simple operations that can detect important regions quickly and efficiently. Each layer can be distorted by the effect of the disease. Our method can estimate the distortion rate and possible normal layer boundary, which may be useful for doctors. This feature of our algorithm makes it special, whereas the above-mentioned algorithms cannot estimate the boundary of a normal layer.

2 Methods

Now, we will present our proposed method for detecting boundary layers and subretinal fluid regions. The procedure first delineates the inner and outer boundary retinal layers (ILM and RPE, resp.) using vertical profiles of OCT cross-section images. Then subretinal fluid regions are localized and delineated. This is followed by calculating quantitative measures such as the extent of subretinal fluid in each slice, thickness and creasing of retinal layers. Once we have this information for each slice, other (regional or global) metrics (e.g. subretinal fluid volume) can also be readily computed.

2.1 ILM and RPE layer extraction

The OCT images are affected by distortions like "shadowing" by blood vessels, and these may lead to false detections. First, we improve the image quality by noise filtering and contrast enhancement using a fuzzy operator [4]. This can highlight major retinal layers. We analyze vertical profiles of the filtered image and large intensity steps in pixel density are assumed to correspond to change in tissue. The function is defined by the expression

$$\kappa_\nu^* = \frac{1}{1 + \frac{1-\nu}{\nu} \left(\frac{1-x}{x} \frac{\nu}{1-\nu} \right)^\lambda} , \tag{1}$$

where ν is the threshold, x is the pixel intensity and λ denotes sharpness of the filtering. As we mentioned earlier, the κ_ν^* function can highlight boundary layers and help suppress noise. We determined dynamically the input parameter ν in a simple way. We sampled from the top range of the image and calculated the average intensity for this ROI. The λ parameter value was set to 3, empirically. Figure 2 shows an example where the κ_ν^* function was applied.

After filtering, we divided the image into bars with fixed width. A bar consisted of 10 consecutive pixel columns and we calculated the horizontal projections of each
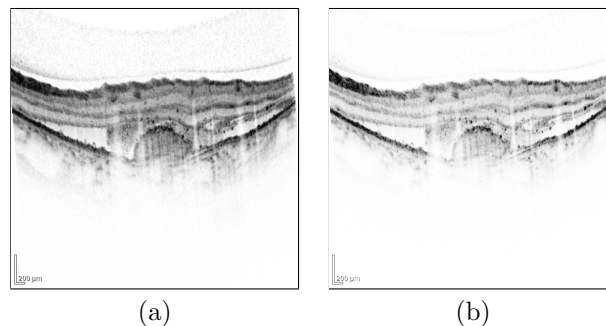

(a) (b)

Figure 2: Sample OCT image before (a) and after (b) applying the κ_ν^* function.
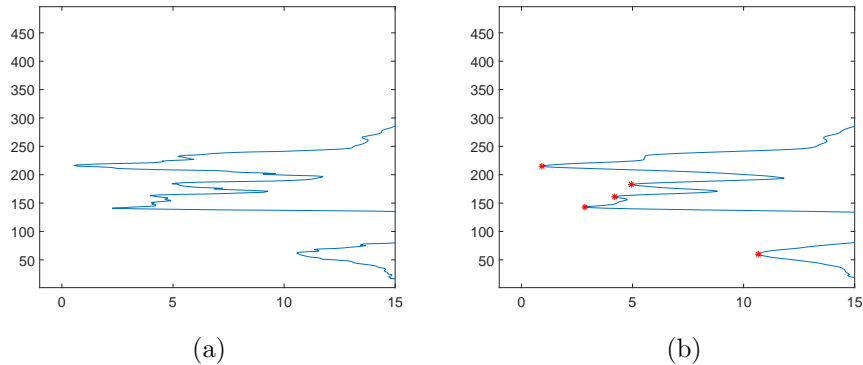
Figure 3: Calculated horizontal projection of a bar (a) and the Savitzky-Golay filtered data (b).

bar to determine the boundaries. One of the major steps of our proposed procedure is to analyze the vertical profiles. As this signal was noisy, it was necessary to filter the data. We used the Savitzky-Golay filter [18], which is a smoothing digital filter. This filter is good at preserving the relevant high frequency components of the signal, which is an important aspect for our detection method. In Fig. 3, there is an example of a projection (Fig. 3(a)) and its filtered version (Fig. 3(b)).

To determine of the outer layer boundary is harder than the inner boundary, because Choriocapillaris and Chorodoidal vessels are located under the RPE layer. The intensity of these regions vary, so several peaks appear in the projections. Fortunately, in most cases, these minimum points are not prominent, and do not cause a problem in the choice of the right locations. The algorithm chooses the outstanding local minimum from the projected data to identify the possible inner and outer layers.

Some of our OCT image volumes are strongly affected by noise or blood vessels shadows. To achieve a more efficient and reliable segmentation, we need to estimate the artifacts caused by the blood vessels. Below, we describe a method for detecting blood vessels from the region of interest (ROI), so we have information about the position of retinal blood vessels for each slice, which will aid layer boundary detection.

2.2 Blood vessel segmentation

Now, we summarize our simple approach for segmenting retinal blood vessels in fundus images. Fundus images are also provided with the OCT studies, in addition to the cross-section slices, and spatial correspondence is well defined. Hence we can use the fundus image for vessel segmentation and later use this information when processing the OCT slices.

Major vessels cause a bigger shadowing effect on the OCT slices than the minor

capillaries. Here, we do not seek to have a perfect segmentation of the whole vessel tree. The segmentation output will be used to identify those positions (bars) on the OCT slices where shadowing may be significant, since this can invalidate our underlying assumption about large intensity steps matching layer boundaries. Once we can localize these less reliable parts of the image, we can specially treat (or even exclude) these parts from the layer boundary detection algorithm and handle them as "missing data" rather than using "false information".

Many published methods in the literature [6] deal with the retina vessel segmentation problem and try to achieve the most accurate segmentation possible. For our purposes, a rough estimate is sufficient, as the vessels are not the objective of our studies, they merely locally spoil the contrast which hinders layer detection. It can be seen in Fig. 4(a) that the central region (the macula and its surrounding) is significantly darker than other parts of the image, hence the contrast between blood vessels and their surrounding background differs in the central and the peripherical parts of the image. Here our aim is to localize these regions and homogenize them in a simple way. For this, we use a Gaussian-pyramid technique with 4 levels. Figure 4(b)) depicts one level of the pyramid. Intensity homogenization is performed as a pixel operator according to the following formula:

$$I_{(x,y)} = C \cdot I_B(x,y)/I_O(x,y) \text{ for all pixels } (x,y) \text{ in the image} , \qquad (2)$$

where I_O is the original image, I_B is the blurred image, and C is the maximal intensity in I_O. Figure 4(c) shows the result of applying (2).

Intensity homogenization is followed by a contrast enhancement step, using an adaptive fuzzy contrast stretching method, which is more effective than a commonly used contrast stretching procedure. Let I denote the input image, I_{max} the maximum intensity and I_{min} the minimum intensity of the image. The linear membership function $\mu_{i,j}$ is defined as

$$\mu_{i,j} = (I_{i,j} - I_{min})/(I_{max} - I_{min}) , \qquad (3)$$

i.e., the membership value for pixel (i,j) corresponds to the degree of brightness of the gray level intensity of that pixel relative to the intensity range of the whole image. This is a simple way to assign fuzzy membership values to elements of a set (to the pixels, in our case). In a fuzzy processing approach, memberships are manipulated instead of original properties. We achieve contrast enhancement by using the intensification operator (INT) [17]

$$\mu'_{i,j} = \begin{cases} 2 \cdot (\mu_{i,j})^2, & \text{if } 0 \leq \mu_{i,j} \leq T , \\ 1 - 2 \cdot (1 - \mu_{i,j})^2, & \text{otherwise} , \end{cases} \qquad (4)$$

where T is an adaptively calculated threshold value. We used the statistical mean of the intensities in each window to calculate T. Eq. (4) transforms membership values that are above the threshold to values that are much higher and membership values that are lower than the threshold to values that are much lower, in a nonlinear manner. The last step here is defuzzification, i.e., generating properties in the
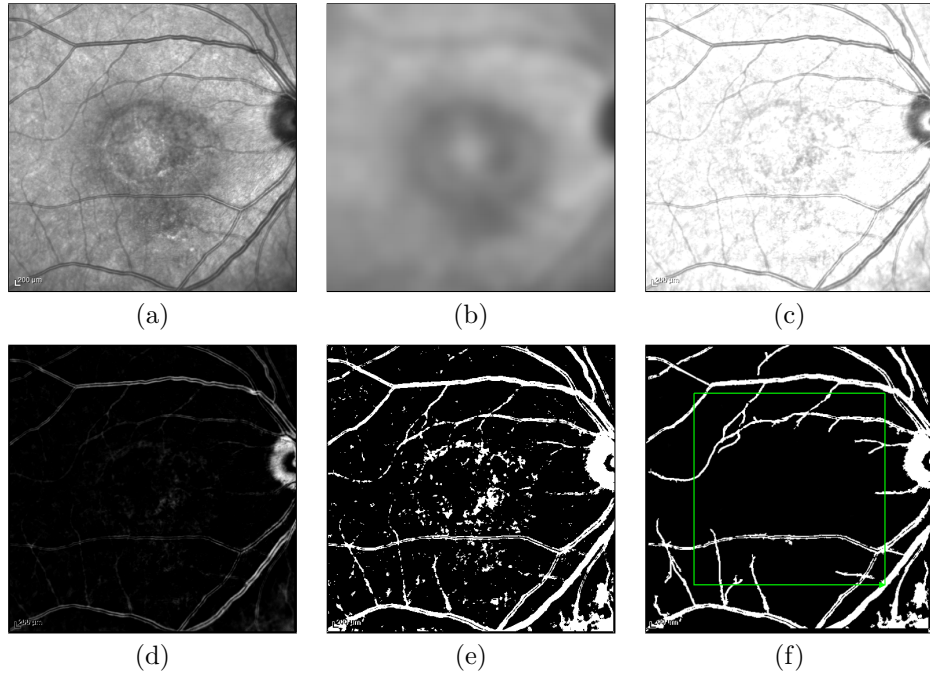
Figure 4: Main steps of retinal blood vessel segmentation: (a) original image, (b) one level of the Gaussian-pyramid, (c) homogenization, (d) fuzzy contrast stretching (in complementer image), (e) binarization, (f) output image (after removal of false objects).

original dimensions from the resulted memberships. $I'_{i,j}$ denotes the calculated new intensity for pixel (i,j), and it is got by applying the inverse of the transformation used for fuzzification:

$$I'_{i,j} = I_{min} + \mu'_{i,j} \cdot (I_{max} - I_{min}) . \tag{5}$$

Figure 4(d) illustrates the contrast enhanced image. The contrast enhanced image is turned into binary values in order to extract possible blood vessel regions, using adaptive thresholding in a sliding 15×15 window. In the next step, we eliminate false positive objects, because vessels constitute a connected object, so smaller segments perhaps arise from noise. We use morphological closing with a rectangle shaped structure element. The size of the element is consistent with the thinnest blood vessel. Afterwards, we reject all those regions whose area is less than 10 pixels and whose shape is not elongated. Once we have the vessel mask on the fundus image, we can project these data values onto the OCT cross-sections.

2.3   Automatic detection of subretinal fluid

Before turning to the subretinal fluid regions, we will assume that blood vessels and the ILM and RPE boundaries are already found in each OCT slice. Our procedure uses these data values when estimating subretinal fluid regions. Subretinal fluid is close to the RPE layer and appears as a larger hyporeflective connected component. For processing, we use the negative of signals, because our medical colleagues use the inverted presentation of images for the visual assessment and also exported the image data for us in this format. When layers are very creased due to AMD, these regions split up into multiple objects. To localize the fluid, we first use the Savitzky-Golay filtered signal that was introduced in Section 2.1. Once again, we process the OCT slices in vertical stripes, and based on the above assumptions, we look for minimum locations on the horizontal projections that are closest to the RPE layer. Some outliers can be filtered out based on assumptions about the layer thickness. Using the vessel shadow information, we can filter out those stripes that are less reliable than the others, and fit a smooth curve to the reliably detected minimum locations, thus approximating the fluid surface in the less reliable positions. In Section 2.1, we recommended a possible normal outer layer boundary. This can help us to define the degree of creasing of the layers and it also supports outlier filtering. These conditions reduce the dataset sufficiently, so after this step, we can fit a curve to the detected points and outline the subretinal fluid region.

3   Evaluation

3.1   Image data

Our evaluation dataset contained 11 Heidelberg Spectralis OCT scans of wet age-related macular degeneration patients treated with anti-VEGF intravitreal injections. The scanning parameters were: a 49 scan pattern, a pattern size of 5.8×5.8 mm, a distance between B-scans of $121\,\mu$m, a size X of 512 pixels, a size Z of 496 pixels; the pixel size was $11.44\,\mu$m and $3.87\,\mu$mm in X and Z directions, respectively.

Manual ILM and RPE layer segmentation was performed by ophthalmologists for 7 image sequences. This was treated as the ground truth for evaluating the boundary layer detection method on these 7 volumes.

3.2   Results and discussion

The proposed method was implemented in MATLAB, with the help of the Image Processing Toolbox. We evaluated our retinal layer detection algorithm in two different ways. Firstly, to compare the results of our algorithm against the manual delineations, we calculated the mean, maximum and standard deviation of boundary errors for every surface. The 7 curves shown in Figure 5 depict the error histogram for those OCT volumes where manual annotation was available. Each curve aggregates the boundary errors in the 49 scans (slices) of a study.
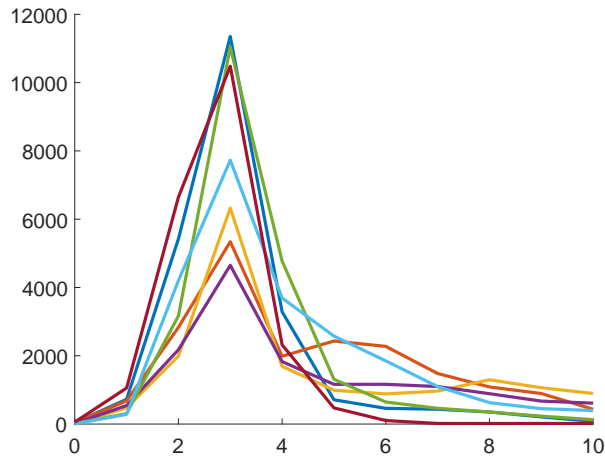
Figure 5: Error histogram of 7 image sequences.

Table 1: Summary of the mean, standard deviation, and maximum error (in pixels) between manually segmented and automatically detected layers in 7 annotated OCT image sequences.

	Mean	Standard deviation	Maximum
Seq_02	2.01	1.56	17
Seq_03	2.10	0.69	15
Seq_04	1.44	0.65	15
Seq_05	1.96	0.80	19
Seq_06	2.39	1.63	18
Seq_07	2.17	0.64	15
Seq_08	1.83	0.65	17
All	1.98	0.94	16.57

It shows that the highest error measure is between 1 and 4 pixels in most cases and Table 1 asserts to this statement. As shown in Table 1, the maximal distance between manually segmented and automatically detected layer boundary is 19 pixels (ca. $73.5\,\mu$m). This deflection comes from two sources: the substantial jumps between B-scans and layer distortions due to the disease. Unfortunately, we could not exploit 3D information directly to segment layers because there are some anomalies among slices of the OCT volume, due to the image acquisition and registration process (within the device's software).

Secondly, as you can see in the right-hand example in Figure 6, there is a big difference between the manually annotated and the automatically segmented outer
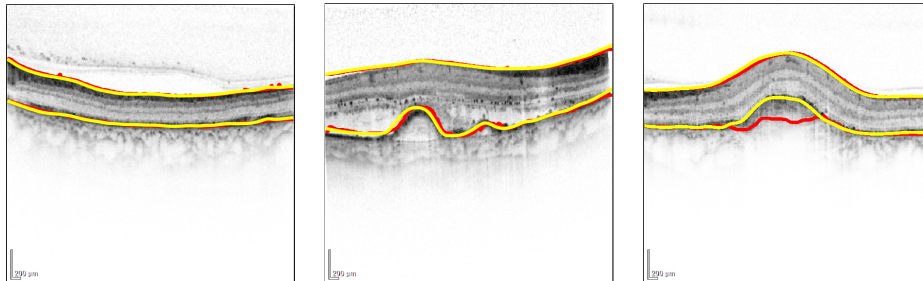
Figure 6: Visual comparison of expert annotated (in red) and automatically detected (in yellow) layers.

layer because our algorithm follows the distorted layers. Still, the recommended possible normal boundary aligns well with the manual annotation, so it avoids the false detection. Nevertheless, in most cases, the mean errors are less than 2 pixels and deviations are small between layers delineated by medical experts and the boundaries determined automatically, hence the difference is usually negligible.

In Section 2.3, we proposed a method for the automatic detection of subretinal fluid. Unfortunately, expert annotation was not yet available for the quantitative evaluation on a larger set of cases. Figure 6 illustrates the performance of the algorithm in a qualitative manner, presenting some example scans with overlaid manual layer segmentation.

The main advantage of our proposed method is its simplicity, i.e. it uses simple images processing operations which can be parallelized, and it does not need lots of parameters that are difficult to tune to the application (in contrast to the energy minimization approach, say).

Automatically calculated quantitative descriptors may be graphically presented to the reader to aid interpretation of data. The first is a traditional slice-by-slice display which provides a good depth context within a slice, but no spatial context between slices. In a colored overlay (image fusion), an anatomical display offers regional context and color encodes quantitative parameters. Figure 7 shows a restricted subretinal fluid area where the results were verified by ophthalmologists and they said that they the segmentation, quantification and also the visualization technique quite useful.

4   Concluding remarks

Here, we presented an algorithm for the detection of subretinal fluid areas and retinal layers and we presented some visualization techniques to illustrate the result. We calculated metrics to quantify features of the OCT from the perspective of AMD patients. After seeing the results, medical doctors at our clinic think that digital image processing can help in the quantitative assessment of the OCT features of AMD by providing automatic tools that can detect abnormalities and describe via
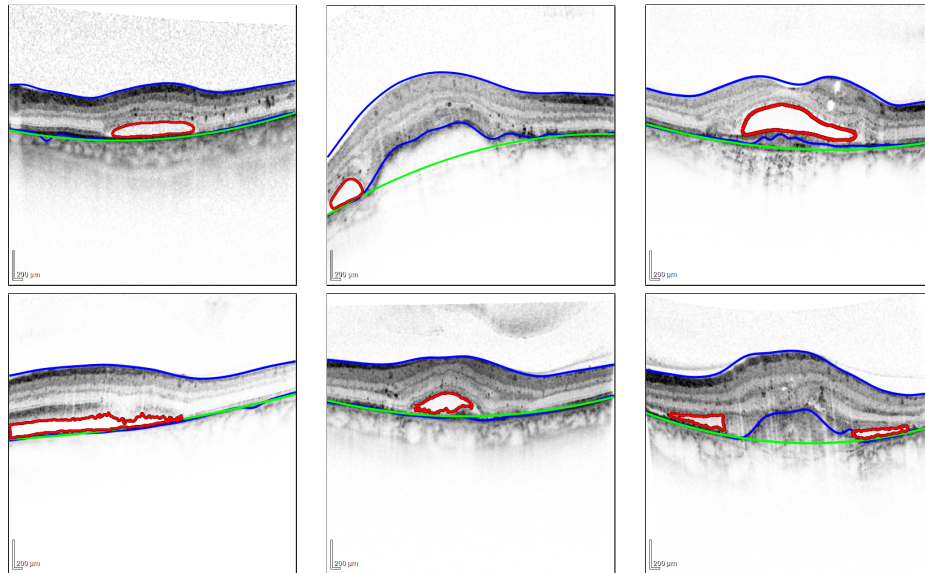
Figure 7: An illustration of detected boundaries and quantitation. The blue curves represent the detected boundaries, the green curve is the fitted normal layer boundary and the red curve shows the detected fluid volume boundary.
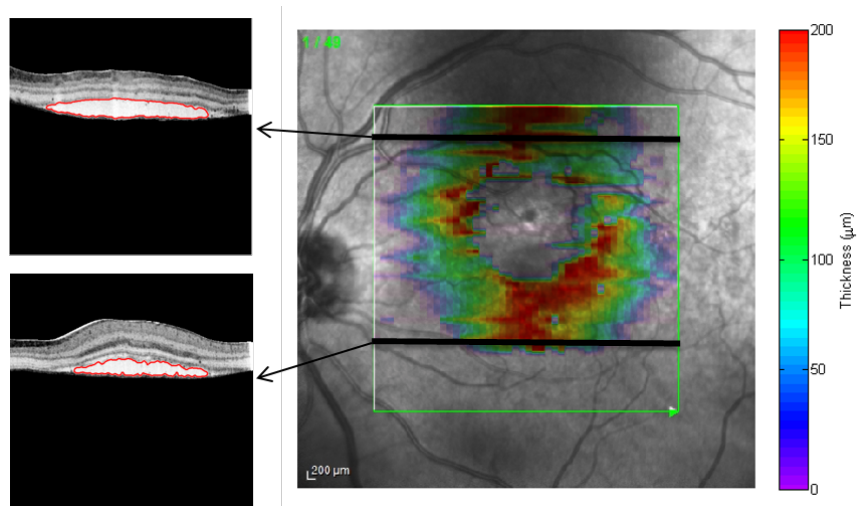

Figure 8: Color overlay of the subretinal fluid volume thickness. Left: The red boundaries indicate the subretinal fluid in each slice. Right: The color/hue represents subretinal fluid thickness.

objective metrics the current state of the disease and longitudinal changes during treatment. Using SD-OCT to follow up changes of subretinal fluid volume will become a useful tool for detecting subtle changes during the course of treatment. Further studies are planned in order to evaluate these new tools in a cohort of AMD patients.

Acknowledgements

References

[1] Abhishek, A. M., Berendschot, T. T. J. M., Rao, S. V., and Dabir, S. Segmentation and analysis of retinal layers (ILM & RPE) in Optical Coherence Tomography images with Edema. In *Biomedical Engineering and Sciences (IECBES), 2014 IEEE Conference on*, pages 204–209, 2014.

[2] Chiu, S. J., Li, X. T., Nicholas, P., Toth, C. A., Izatt, J. A., and Farsiu, S. Automatic segmentation of seven retinal layers in SDOCT images congruent with expert manual segmentation. *Optics Express*, 18(18):19413–19428, 2010.

[3] Ding, W., Young, M., Bourgault, S., Lee, S., Albiani, D. A., Kirker, A. W., Forooghian, F., Sarunic, M. V., Merkur, A. B., and Beg, M. F. Automatic detection of subretinal fluid and sub-retinal pigment epithelium fluid in optical coherence tomography images. In *2013 35th Annual International Conference of the IEEE Engineering in Medicine and Biology Society (EMBC)*, pages 7388–7391, 2013.

[4] Dombi, J. *Modalities*, pages 53–65. Springer Berlin Heidelberg, 2012.

[5] Ferrara, N. Vascular endothelial growth factor: Basic science and clinical progress. *Endocrine Reviews*, 25(4):581–611, 2004.

[6] Fraz, M. M., Remagnino, P., Hoppe, A., Uyyanonvara, B., Rudnicka, A. R., Owen, C. G., and Barman, S. A. Blood vessel segmentation methodologies in retinal images a survey. *Computer Methods and Programs in Biomedicine*, 108(1):407–433, 2012.

[7] Fu, D., Tong, H., Luo, L., and Gao, F. Retinal automatic segmentation method based on prior information and optimized boundary tracking algorithm. In *Proc. SPIE*, volume 10033, pages 100331C:1–100331C:6, 2016.

[8] Garvin, M. K., Abramoff, M. D., Wu, X., Russell, S. R., Burns, T. L., and Sonka, M. Automated 3-D Intraretinal Layer Segmentation of Macular Spectral-Domain Optical Coherence Tomography Images. *IEEE Transactions on Medical Imaging*, 28(9):1436–1447, 2009.

[9] Goldstein, Tom, Bresson, Xavier, and Osher, Stanley. Geometric applications of the split Bregman method: Segmentation and surface reconstruction. *Journal of Scientific Computing*, 45(1):272–293, 2010.

[10] Hassan, B., Raja, G., Hassan, T., and Akram, M. U. Structure tensor based automated detection of macular edema and central serous retinopathy using optical coherence tomography images. *Journal of the Optical Society of America*, 33(4):455–463, 2016.

[11] Hee, M. R., Baumal, C. R., Puliafito, C. A., Duker, J. S., Reichel, E., Wilkins, J. R., Coker, J. G., Schuman, J. S., Swanson, E. A., and Fujimoto, J. G. Optical Coherence Tomography of Age-related Macular Degeneration and Choroidal Neovascularization. *Ophthalmology*, 103(8):1260–1270, 1996.

[12] Kovach, J. L., Schwartz, S. G., Jr., H. W. Flynn, and Scott, I. U. Anti-VEGF treatment strategies for wet AMD. *Journal of Ophthalmology*, 22:786870:1–786870:7, 2012.

[13] Lang, A., Carass, A., Hauser, M., Sotirchos, E. S.and Calabresi, P. A., Ying, H. S., and Prince, J. L. Retinal layer segmentation of macular OCT images using boundary classification. *Biomedical Optics Express*, 4(7):1133–1152, 2016.

[14] Lim, J.I. *Age-Related Macular Degeneration*. CRC Press, 2012.

[15] Lu, S., l. Cheung, C. Y., Liu, J., Lim, J. H., s. Leung, C. K., and Wong, T. Y. Automated layer segmentation of optical coherence tomography images. *IEEE Transactions on Biomedical Engineering*, 57(10):2605–2608, 2010.

[16] Novosel, J., Wang, Z., de Jong, H., van Velthoven, M., Vermeer, K. A., and van Vliet, L. J. Locally-adaptive loosely-coupled level sets for retinal layer and fluid segmentation in subjects with central serous retinopathy. In *2016 IEEE 13th International Symposium on Biomedical Imaging (ISBI)*, pages 702–705, 2016.

[17] Pal, S. K. and King, R. A. Image enhancement using smoothing with fuzzy sets. *IEEE Transactions on Systems, Man, and Cybernetics*, 11(7):494–501, 1981.

[18] Schafer, R. W. What Is a Savitzky-Golay Filter? *IEEE Signal Processing Magazine*, 28(4):111–117, 2011.

[19] Wang, J., Zhang, M., Pechauer, A. D., Liu, L., Hwang, T. S., Wilson, D. J., Li, D., and Jia, Y. Automated volumetric segmentation of retinal fluid on optical coherence tomography. *Biomedical Optics Express*, 7(4):1577–1589, 2016.

[20] Xu, X., Lee, K., Zhang, L., Sonka, M., and Abrmoff, M. D. Stratified sampling voxel classification for segmentation of intraretinal and subretinal fluid in longitudinal clinical OCT data. *IEEE Transactions on Medical Imaging*, 34(7):1616–1623, 2015.

[21] Yazdanpanah, A., Hamarneh, G., Smith, B., and Sarunic, M. *Intra-retinal Layer Segmentation in Optical Coherence Tomography Using an Active Contour Approach*, pages 649–656. Springer Berlin Heidelberg, 2009.

[22] Zheng, Y., Sahni, J., C. Campa, A. N. Stangos, A. Raj, and Harding, S. P. Computerized Assessment of Intraretinal and Subretinal Fluid Regions in Spectral-Domain Optical Coherence Tomography Images of the Retina. *American Journal of Ophthalmology*, 155:277–286, 2012.